Journal of Alloys and Compounds 586 (2014) 136–141

Contents lists available at ScienceDirect

Journal of Alloys and Compounds

journal homepage: www.elsevier.com/locate/jalcom

Novel X7R $BaTiO_3$ ceramics co-doped with La^{3+} and Ca^{2+} ions

D.-Y. Lu *, Y. Yue, X.-Y. Sun

Research Center for Materials Science and Engineering, Jilin Institute of Chemical Technology, Jilin 132022, China

ARTICLE INFO

Article history:
Received 10 August 2013
Received in revised form 2 October 2013
Accepted 7 October 2013
Available online 18 October 2013

Keywords:
Ceramics
Pseudo-cubic
Defect complexes
Dielectric response
X7R
Raman charge effect

ABSTRACT

$(Ba_{1-x}La_x)(Ti_{1-x/2}Ca_{x/2})O_3$ ($0.03 \leqslant x \leqslant 0.06$) (BLTC) ceramics were prepared using a mixed oxides method. The structure, microstructure, and dielectric properties of BLTC were investigated by X-ray diffraction, Raman spectroscopy, scanning electron microscopy, atomic force microscope, and dielectric measurements. Both symmetric (200) XRD peak indicative of cubicity and sharp 308 cm^{-1} Raman band indicative of tetragonality are characteristics of pseudo-cubic symmetry of BLTC. The unit cell volume of BLTC increased linearly with x, satisfying Vegard's law. A strong "Raman charge effect" appeared at 836 cm^{-1} because of the aliovalent double substitution in BLTC. The $x = 0.03$ sample because of its higher permittivity ($\varepsilon' = \sim 2000$) and lower loss ($\tan\delta < 0.04$) is a novel dielectric for X7R applications. The formation of $La_{Ba}^{\cdot} - Ca_{Ti}'' - La_{Ba}^{\cdot}$ defect complexes was responsible for the dielectric-temperature stability of BLTC.

1. Introduction

In the dielectric field of $BaTiO_3$-based ceramic materials, the two typical dielectric specifications named by the Electronic Industry Association (EIA) are Y5V ($-82\% \leqslant (\varepsilon' - \varepsilon'_{RT})/\varepsilon'_{RT} \leqslant +22\%$ in a temperature range −30 to 85 °C) and X7R ($|(\varepsilon' - \varepsilon'_{RT})/\varepsilon'_{RT}| \leqslant 15\%$ in a range −55 to 125 °C). They represent room-temperature high-ε (i.e., high-k) behavior and dielectric-temperature stability, respectively. It is well known that the Curie temperature (T_C) of $BaTiO_3$ is approximately 125 °C, at which a clear cubic-tetragonal phase transition occurs, accompanied by a very sharp dielectric peak ($\varepsilon' \sim 10{,}000$) [1,2]. This phase transition belongs to a first-order phase transition (FPT) [3]. In most cases, when $BaTiO_3$ is doped with different types of ions, its T_C generally shifts toward low temperature, and with increasing doping levels, this sharp dielectric peak gradually becomes vague, forming so-called diffuse phase transition (DPT) [3]. Because the reduplicative orientations by TiO_6 octahedron constitute the skeleton of the $BaTiO_3$ perovskite structure and Ba ions are located on the interstitial space of the TiO_6 skeleton [4], the substitution of dopants at the Ti site compared to the Ba site will induce a larger lattice deformation, which can cause a stronger broadening of the permittivity maximum (ε'_m) associated with DPT. The Y5V specification needs DPT to occur as far as possible in the vicinity of room temperature. This requires that the solid solution limit of dopants at the Ti site in the $BaTiO_3$ lattice is sufficiently high to enable the ε'_m to shift to room temperature.

The ionic radius of dopants is a critical factor contributing to DPT. The radii of some ions versus coordinate number (CN) are listed in Table 1 [5]. Three types of Ti-site dopants such as Sn^{4+} (0.69 Å), Zr^{4+} (0.72 Å), and Ce^{4+} (0.87 Å), are illustrated to focus on the relationship between the ionic size of dopants and DPT. These three dopants have higher Ti-site solid solubility because of their high ability to maintaining the lattice electroneutrality [3,6–8]. One found that with an increase in ionic radius, the sintering temperature needs to be elevated continuously so that the doping ions gain enough energy to enter the Ti site of the BO_6 octahedrons skeleton, and that the phase transition becomes more diffused, as observed for Ce^{4+}-doped $BaTiO_3$ [8]. Although these $BaTiO_3$-based ceramics might meet Y5V or Z5U ($-56\% \leqslant (\varepsilon' - \varepsilon'_{RT})/\varepsilon'_{RT} \leqslant +22\%$ in a range 10–85 °C) specifications [3,6–8], they cannot reach the X7R specification. One probably imagines that with increasing the size of Ti-site doping ions, a continuous trend of the ε'_m smoothness would be going on, accompanied by an evolution from Y5V-type high-ε behavior to X7R-type dielectric-temperature stability.

However, it is difficult to find an ideal Ti-site tetravalent dopant whose ionic radius is greater than Ce^{4+}. In recent years, Zhang et al. proposed Ti-site Ca^{2+} (1.00 Å) as a potential dopant for applications of a higher dielectric specification X8R ($|(\varepsilon' - \varepsilon'_{RT})/\varepsilon'_{RT}| \leqslant 15\%$ in a range −55 to −155 °C) [9]. The much larger ionic size of Ca^{2+} (1.00 Å) compared to Ti^{4+} (0.605 Å) results in a lower Ti-site solid solution limit of $x = \sim 0.04$ for $Ba(Ti_{1-x}Ca_x)O_{3-x}$ with DPT at $T_C = 44$ °C, and the sintering temperature had to be elevated to a higher temperature of 1500 °C [9]. Even so, researchers cannot achieve the Y5V specification for $Ba(Ti_{1-x}Ca_x)O_{3-x}$. This is probably

* Corresponding author. Tel.: +86 13944220469.
E-mail addresses: cninjp11232000@yahoo.com, dylu@jlict.edu.cn (D.-Y. Lu).

0925-8388/$ - see front matter © 2013 Elsevier B.V. All rights reserved.
http://dx.doi.org/10.1016/j.jallcom.2013.10.055

Table 1
Ionic radii versus coordinate number (CN).

Ion	CN	r (Å)
Ba^{2+}	12	1.61
Ti^{4+}	6	0.605
La^{3+}	12	1.36
Ca^{2+}	12	1.34
Ca^{2+}	6	1.00
Ce^{4+}	6	0.87
Zr^{4+}	6	0.72
Sn^{4+}	6	0.69

attributed to the presence of oxygen vacancies caused by the aliovalent substitution of Ca^{2+} at the Ti site.

In this work, our purpose is to incorporate much larger Ca^{2+} ions completely into the Ti site by means of Ba-site codopant in $BaTiO_3$, to achieve a more diffused phase transition and further to expect X7R-type dielectric-temperature stability. La^{3+} donor (an ion with a higher valence than the host Ba^{2+} ion) and Ca^{2+} acceptor (an ion with a lower valence than the host Ti^{4+} ion) are used as codopants at the Ba- and Ti-sites in $BaTiO_3$, respectively, to develop $(Ba_{1-x}La_x)(Ti_{1-x/2}Ca_{x/2})O_3$ ceramics, for the three considerations: (1) On the site substitution, Ca^{2+} is generally applied as the Ba-site dopant [10–13]. Even in the case of (Ba + Ca)/Ti = 1, however, Ca-doped $BaTiO_3$ prepared by the mixed oxide route has a feature of the double substitution [14,15]. La ions are known to be substituted exclusively for the Ba site as La^{3+} [16–19]. La^{3+} donor might compel Ca^{2+} as an acceptor to enter the Ti site and then improve the solid solubility of Ca^{2+} at the Ti site. (2) For $Ba(Ti_{1-x}Ca_x)O_{3-x}$, Ca^{2+} in place of Ti^{4+} inevitably induces oxygen vacancies [9,20,21]. The presence of mobile oxygen vacancies is apt to cause electrical conduction and ferroelectric aging. Incorporation of La^{3+} into the Ba site in $Ba(Ti_{1-x}Ca_x)O_{3-x}$ is likely to result not only in reduction of oxygen vacancies and dielectric loss, but also in significant lowering of the sintering temperature by means of the formation of $La_{Ba}^{\cdot} - Ca_{Ti}^{''} - La_{Ba}^{\cdot}$ defect complexes described in Eq. (1), where the Kröger–Vink defect notation [22] is used and the charge equilibrium is equivalent to the host cations, meeting the lattice electroneutrality.

$$La_2O_3 + CaO + TiO_2 \rightarrow 2La_{Ba}^{\cdot} + Ca_{Ti}^{''} + Ti_{Ti} + 6O_O \quad (1)$$

The probable reasons that the formation of defect complexes would lower the sintering temperature are that, a complementary ionic radii relation between $(R_{La} + R_{Ca})$ and $(R_{Ba} + R_{Ti})$ (Table 1) is beneficial to the incorporation of $La_{Ba}^{\cdot} - Ca_{Ti}^{''} - La_{Ba}^{\cdot}$ defect complex as a corporate entity into the perovskite grains, which could surmount the potential barrier of the much larger Ca^{2+} ions entering the Ti site. Meanwhile, at a lower temperature of 1350 °C, La^{3+} ions may induce Ti vacancies [17], which can compel Ca^{2+} ions to enter the Ti site and accelerate diffusion of Ca^{2+} ions into the perovskite grains.

(3) For $BaTiO_3$ ceramics with the double substitution, La^{3+} at the Ba site may play a role in raising dielectric permittivity and further broadening of the ε'_m [23–26].

In this article, we report the results of a comprehensive study of $(Ba_{1-x}La_x)(Ti_{1-x/2}Ca_{x/2})O_3$ (BLTC) solid solution materials. The effect of La/Ca co-doping on structure, microstructure, and dielectric properties are reported. Novel X7R-type dielectric-temperature stability can be realized at a low doping level of $x = 0.03$. Further, there are two advantages of BLTC materials over the conventional X7R $BaTiO_3$-based materials with core–shell structure [27–29]: (1) the control of preparation conditions of BLTC compared to core–shell ceramics is easier; and (2) the X8R specification with higher dielectric-temperature stability can be achieved by La/Ca co-doping at a higher doping level of $x = 0.06$.

2. Experimental procedures

Ceramic raw materials were reagent-grade $BaCO_3$, La_2O_3, TiO_2, and $CaCO_3$ powders. The ceramics were prepared according to the nominal formula $(Ba_{1-x}La_x)(Ti_{1-x/2}Ca_{x/2})O_3$ ($x = 0.03$, 0.04, 0.05, 0.06) (BLTC) using a mixed oxides method described elsewhere [22]. The stoichiometric mixture in accordance with the above formula was carefully mixed. The schedules of calcination, forming (PVA aqueous solution was added as a binder for forming process) and final sintering were at 1100 °C for 5 h in air, 200 MPa for 2 min, and at 1400 °C for 12 h in air, respectively. For the final sintering, the hearting rate was 100 °C/h; the samples were cooled to 1000 °C at a rate of −200 °C/h and then furnace-cooled to room temperature. In addition, $BaTiO_3$ ceramic was prepared at 1300 °C for analysis on lattice deformation of BLTC.

Powder X-ray diffraction (XRD), using a DX-2700 X-ray diffractometer (Dandong Haoyuan Inc.), was used for structural measurements and as an indication of phase purity. Lattice parameters and unit cell volume of BLTC were calculated by MS Modeling (Accelerys, Inc.) using Rietveld refinement in Reflex Package and Cu Kα1 radiation (λ = 1.540562 Å). Raman spectroscopy was carried out using a LabRAM XploRA Raman spectrometer (Horiba Jobin Yvon) with a 532 nm laser. A Linkam-600 heating and cooling stage was equipped for temperature-dependent Raman measurements. Microstructural properties were determined using a JSM-6490 scanning electron microscope (SEM) (JEOL) operated at 25 kV and using a CSPM-5000 atomic force microscope (AFM) (Beyuan Nano-instruments Co.). Scanning was carried out in contact mode AFM with a W-type silicon cantilever and the scanning frequency was set at 1.5 Hz. The surfaces of BLTC samples were polished and thermally-etched for observation of microstructure. Temperature dependences of the dielectric permittivity and loss were measured at 1 kHz using a RCL meter (Fluke PM6306).

3. Results

XRD patterns of BLTC are shown in Fig. 1. All the BLTC ceramics exhibited a single-phase perovskite structure (Fig. 1(a)). There is no indication of any secondary phase separating out. The structures of BLTC were determined as pseudo-cubic, as marked by a symmetric (200) peak (Fig. 1(b)). The larger FWHM (full width of half maximum) values (⩾0.27°) in BLTC compared to that in $BaTiO_3$ (0.15°) implied a larger lattice deformation existing in each BLTC sample. The lattice deformation was smallest for $x = 0.05$ (FWHM = 0.27°) and largest for $x = 0.03$ (FWHM = 0.38°) among all the BLTC ceramics.

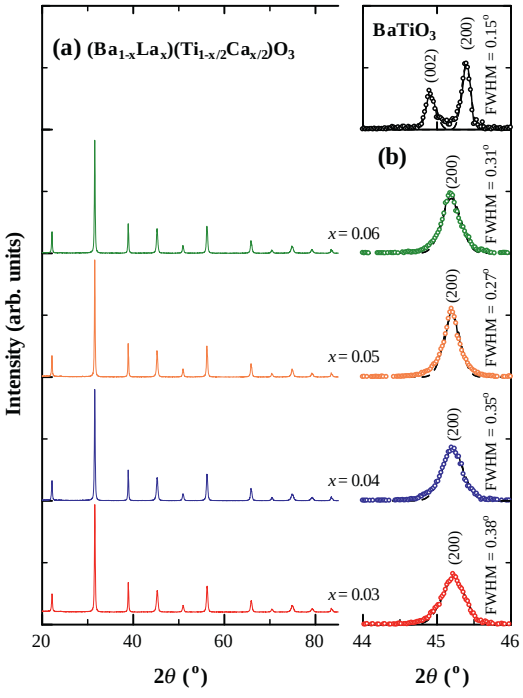

Fig. 1. XRD patterns of (a) $(Ba_{1-x}La_x)(Ti_{1-x/2}Ca_{x/2})O_3$ (BLTC) ceramics ($x = 0.03$–0.06). (b) Gaussian-fitting to the XRD peaks in the vicinity of 45° for BLTC and $BaTiO_3$. FWHM denotes the full width of half maximum of the peak at ~45°.

The variation in unit cell volume (V_0) as functions of x is shown in Fig. 2, where the V_0 values of the tetragonal and cubic $BaTiO_3$ (JCPDS Cards No. 6-526 and 31-174) were drawn as two dashed lines for comparison. The following two facts can give evidence for the formation of $La_{Ba}^{\cdot} - Ca_{Ti}^{''} - La_{Ba}^{\cdot}$ defect complexes: (1) It is well known that Ba-site La^{3+} doping leads to an approximately linear decrease in V_0 [17], whereas Ti-site Ca^{2+} doping leads to an increase in V_0 [9]. The V_0 of BLTC increased linearly with increasing x, which satisfies Vegard's law, i.e., a linear relation exists, at room temperature, between V_0 of the BLTC solid solution and the concentration (x) of combined ($2La^{3+} + Ca^{2+}$) ions. This fact illustrates that the expansion induced by Ca^{2+} ions substituted for the Ti site in TiO_6 octahedrons is greater than the contraction induced by La^{3+} ions located on the interstitial space of the TiO_6 skeleton, although the concentration of La^{3+} was twice that of Ca^{2+}. (2) When x was increased to 0.06, the V_0 of the cubic BLTC was exactly equal to that of the tetragonal $BaTiO_3$ (64.41 Å^3, from JCPDS Cards No. 5-626), but far less than that of the cubic $BaTiO_3$ (65.50 Å^3, from JCPDS Cards No. 31-174). This fact illustrates that the formation of $La_{Ba}^{\cdot} - Ca_{Ti}^{''} - La_{Ba}^{\cdot}$ defect complexes could reduce the cell expansion caused the phase transition from tetragonal to cubic for $BaTiO_3$.

Room temperature measured Raman spectra of BLTC are displayed in Fig. 3. The Raman spectrum of the tetragonal $BaTiO_3$ generally exhibits $B_1 + E$ (TO + LO), A_1 (TO_2), A_1 (TO_3), and A_1 (LO_3) + E (LO_3) optical modes, corresponding to a sharp band at 308 cm^{-1} and three broad bands peaking at 260, 525, and 720 cm^{-1} [7,30]. The band at 308 cm^{-1}, absent in the cubic $BaTiO_3$ [7], is considered as the signature of the tetragonal phase at room temperature. A surprising phenomenon was that this sharp band existed in all the BLTC samples with an average cubic structure determined by XRD. BLTC was therefore pseudo-cubic and the lattice deformation such as orthorhombic or tetragonal existed in the perovskite lattice. The 308 cm^{-1} peak of the sample with $x = 0.05$ was weakest, implying a smallest lattice deformation existed in this sample, in good agreement with the above XRD results.

A band at 836 cm^{-1} appeared in BLTC (Fig. 3). By comparison with the literature [30–32], we can determine whether Ba-site La^{3+} or Ti-site Ca^{2+} could induce this band. Kchikech and Maglione first found this band in La-doped $BaTiO_3$, with an intensity increasing linearly with La content, and considered this band as an indication of the amount of La incorporated into the $BaTiO_3$ lattice [31]. We attributed this phonon mode to an internal deformation of the BO_6 octahedron caused by the charge difference of different types of ions at equivalent sites in $BaTiO_3$ [30], called "Raman charge effect" [33]. Hence, the 836 cm^{-1} band in BLTC can be considered as a combined effect of La^{3+} and Ca^{2+} incorporated into the $BaTiO_3$ lattice. When $x \leqslant 0.05$, the line intensity increased with x. When x was increased to 0.06, however, the line intensity deviated from this linear relationship (Fig. 3 inset).

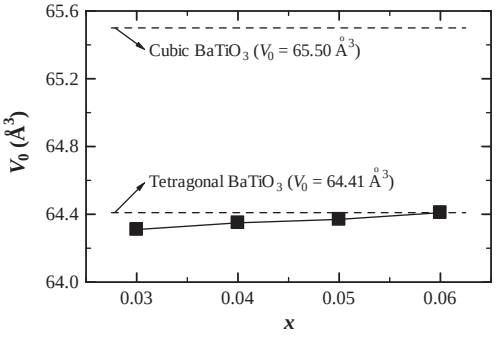

Fig. 2. Plot of the unit cell volume (V_0) as functions of x for BLTC. The data of the tetragonal and cubic $BaTiO_3$ (JCPDS Cards No. 5-626 and 31-174) are given for comparison.

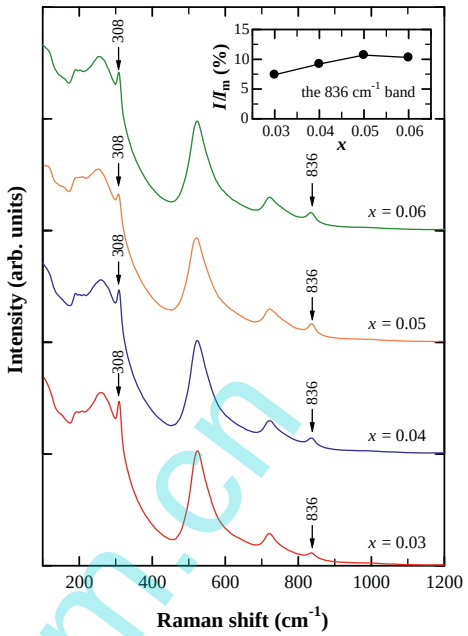

Fig. 3. Room-temperature Raman spectra of BLTC. The inset depicts variation in relative intensity (I/I_m) with x for the 836 cm^{-1} peak. I and I_m represent the band intensities at 836 and 260 cm^{-1}, respectively.

Temperature dependences of the dielectric permittivity (ε') and loss ($\tan\delta$) for BLTC are shown in Fig. 4. All the samples exhibited a little change in dielectric characteristics. The Curie peak of $BaTiO_3$ at T_C = 125 °C was almost completely suppressed because of co-doping with La^{3+} and Ca^{2+}. However, the ε' decreased with increasing x throughout the measuring temperature range. The highest dielectric-temperature stability occurred at $x = 0.06$, satisfying X8R specification. However, this sample exhibited higher dielectric loss ($\tan\delta = \sim 0.06$). The sample with $x = 0.05$ just satisfied X5R specification. Two samples with $x = 0.03$ and 0.04 satisfied X7R

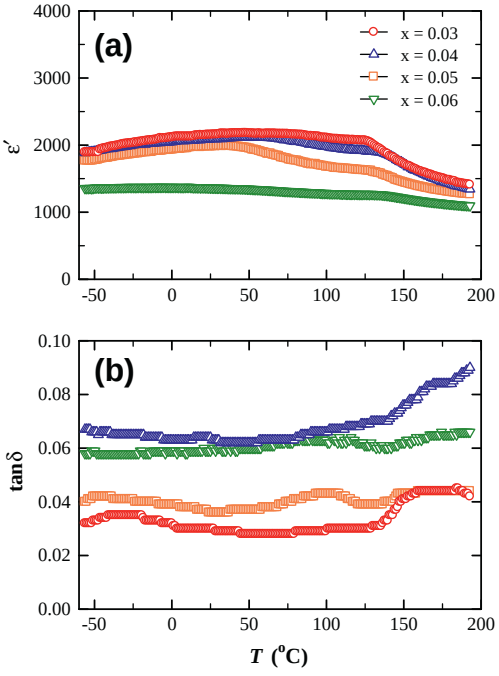

Fig. 4. Temperature dependence of (a) the dielectric permittivity (ε') and (b) the dielectric loss ($\tan\delta$) for BLTC.

specification. The $x = 0.03$ sample is a novel dielectric for X7R applications because of its higher ε' (~2000) and lowest tan δ (<0.04). A weak peak could be observed at ~125 °C for BLTC. This illustrated that the suppressed Curie peak of $BaTiO_3$ could be not shifted by co-doping with La^{3+} and Ca^{2+}.

The above room-temperature Raman results demonstrated that the 308 cm^{-1} band can be considered as the signature of tetragonal or orthorhombic deformation existing in the pseudo-cubic BLTC. The inner lattice deformation in BLTC should be appreciated by means of the evolution of the 308 cm^{-1} band with temperature. For this consideration, the temperature dependent Raman spectra of BLTC were measured, as shown in Fig. 5. Three broad bands at 260, 525 and 720 cm^{-1}, which persisted to 200 °C for each BLTC sample, were attributed to a disorder in the pseudo-cubic phase. The 308 cm^{-1} band disappeared above 125 °C. This fact indicated that the pseudo-cubic phase with tetragonal or orthorhombic distortion at room temperature evolved into a higher cubic symmetry above T_C. The 836 cm^{-1} band associated with Raman charge effect persisted over a measured temperature range, which indicated that the internal deformation of the BO_6 octahedrons caused by the charge difference of dopants existed continuously although BLTC had a higher cubic symmetry at temperatures above T_C = 125 °C.

SEM images of BLTC are shown in Fig. 6. BLTC exhibited a non-uniform microstructure consisting of coarse grains (1–3 μm) and fine grains (~0.7 μm), as seen for the two samples with $x = 0.04$ and 0.06. Here, the average grain size (g) was estimated on a polished plane using Fullman's method [34]. As a reference, the g value of BLTC was determined as 1.6–1.3 μm by averaging the testing values of two coarse-grained pictures and two fine-grained pictures. As a whole, the g decreased with increasing x. For the $x = 0.03$ sample as a valuable candidate for X7R capacitor application, its fine-grained region was investigated with AFM, as shown in Fig. 7. It can be seen that the fine grains was quite homogeneous in the size (g = 0.7 μm). The variations in ceramic density (ρ) and in percentage (P) of ceramic density to the theoretical density as functions of x for BLTC are shown in Fig. 8. The theoretical density calculated using the lattice parameters and molecular weight of BLTC was 6.02–6.01 g/cm^3. Both ρ and P decreased with increasing x, implying that an increased porosity with x might correlate with a decrease in ε' throughout the measuring temperature range.

4. Discussion

4.1. Solid solution formation, defect complexes, and Raman charge effect

It is well known that when the sintering temperature was held at 1500 °C, the solid solution limit of Ca^{2+} at the Ti site in $BaTiO_3$ was approximately 0.04 [9]. By means of co-doping with La^{3+} and Ca^{2+}, a pseudo-cubic BLTC can be prepared at a lower temperature of 1400 °C. This is mainly attributed to the formation of $La_{Ba}^{\cdot} - Ca_{Ti}'' - La_{Ba}^{\cdot}$ defect complexes in BLTC, as described in Eq. (1).

There are two decisive factors responsible for the solid solution formation of BLTC: (1) La^{3+} has priority over Ca^{2+} in the Ba-site occupation. La^{3+} ions were first incorporated into the Ba site to induce Ti vacancies [16–18,23], which could compel Ca^{2+} ions to enter the Ti site and accelerate diffusion of Ca^{2+} ions into the perovskite grains; and (2) two La^{3+} ions next to one Ca^{2+} ion formed a $La_{Ba}^{\cdot} - Ca_{Ti}'' - La_{Ba}^{\cdot}$ defect complex, which could be incorporated as an entity directly into the perovskite grains to relieve BO_6 octahedron expansion caused by the substitution of much larger Ca^{2+} for Ti^{4+}. These two factors concurred throughout the solid solution formation of BLTC. At a lower sintering temperature (1400 °C), the second factor made a great contribution to the solid solution formation of BLTC.

In order to search for the cause of the linear deviation (Fig. 3 inset), the cubic $(Ba_{1-x}Nd_x)(Ti_{1-y}Fe_y)O_3$ (BNTF) ceramics were chosen for Ref. [33]. When the doping levels of Ba-site Nd^{3+} were equal to those of Ti-site Fe^{3+} ($x = y$), $Nd_{Ba}^{\cdot} - Fe_{Ti}'$ defect complexes formed in the $BaTiO_3$ host lattice were charge self-balanced and equivalent to $Ba_{Ba} - Ti_{Ti}$, showing no Raman charge effect; whereas BNTF with $x > y$ showed a similar Raman charge effect [33] to Nd-doped $BaTiO_3$ [35]. On the basis of the fact in BNTF, at a higher doping level such as $x = 0.06$, the deviation from the linear relationship in BLTC might be attributed to an orientation tendency of two La^{3+} ions in $La_{Ba}^{\cdot} - Ca_{Ti}'' - La_{Ba}^{\cdot}$ complex in part along cube diagonal of one cell including CaO_6 octahedron. The Raman charge effect because of those orientations was reduced for $x = 0.06$. Correspondingly, at lower doping levels of $x \leqslant 0.05$, a disorder of La^{3+} and Ca^{2+} ions in orientations was responsible for the linear relationship in BLTC.

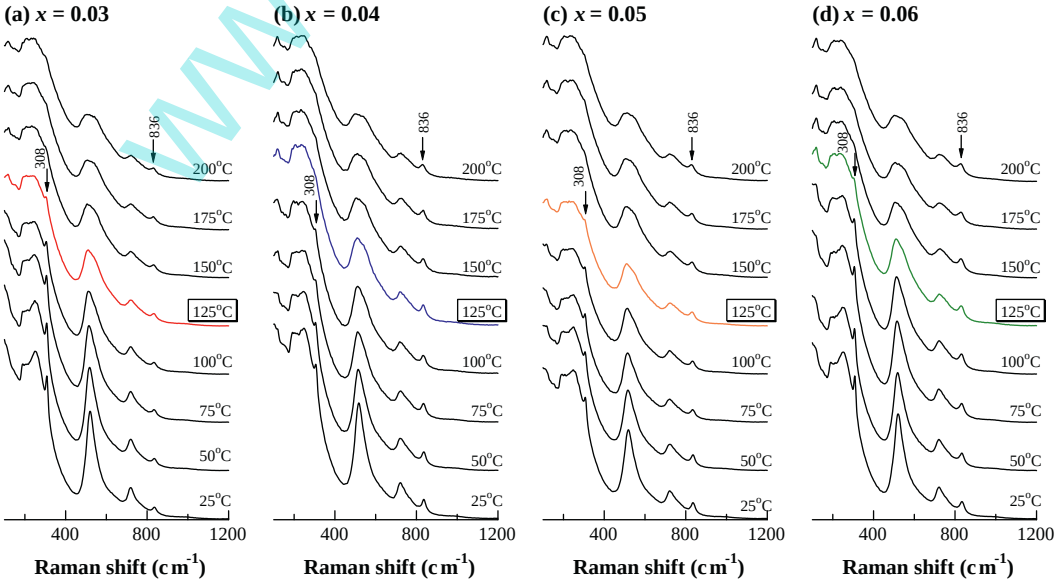

Fig. 5. Temperature dependent Raman spectra of BLTC. (a) $x = 0.03$, (b) $x = 0.04$, (c) $x = 0.05$, (d) $x = 0.06$.

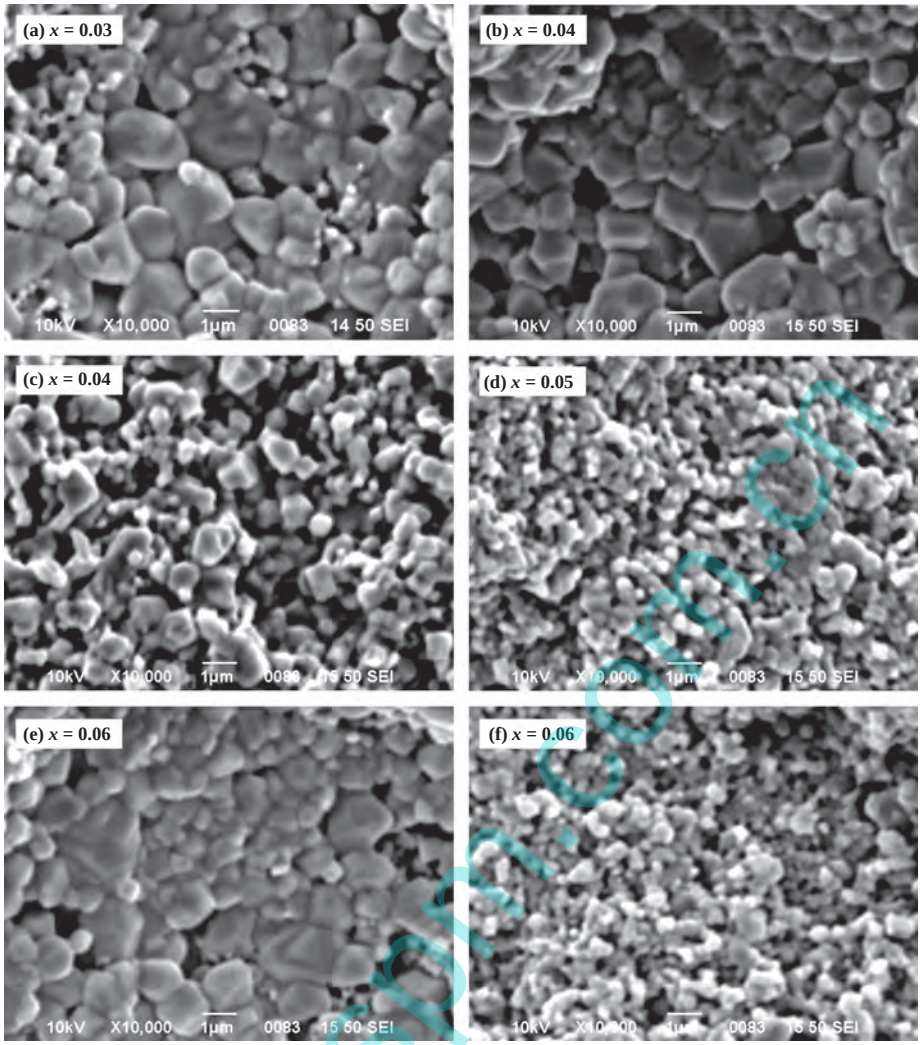

Fig. 6. SEM images of BLTC ceramics with (a) $x = 0.03$, (b) and (c) 0.04, (d) 0.05, and (e) and (f) 0.06.

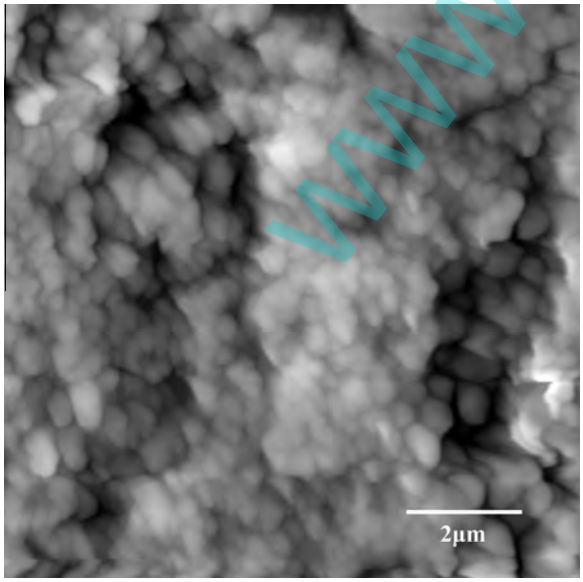

Fig. 7. AFM image for X7R-type BLTC ceramic with $x = 0.03$.

Since the Raman charge effect disappears in the case of $Nd_{Ba}^{\cdot} - Fe_{Ti}^{\prime}$ defect complexes that balance out the charge in BNTF

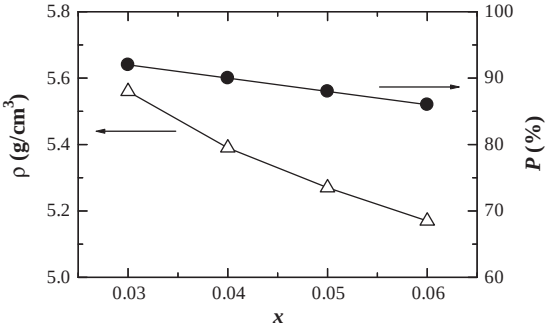

Fig. 8. Variations in ceramic density (ρ) and in percentage (P) of ceramic density to the theoretical density as functions of x for BLTC.

with $x = y$ [33], one should imagine that the Raman charge effect should also not be present for the $La_{Ba}^{\cdot} - Ca_{Ti}^{\prime\prime} - La_{Ba}^{\cdot}$ complexes in BLTC, as their charge is also balanced out. We found that in the case of defect complexes the Raman charge effect is associated with the radius of doping ion at the Ti site. When the size of Ti-site doping ion is less than that of Ti^{4+} (0.605 Å), one Ti-site doping ion (such as Fe^{3+} (0.55 Å) [5]) in the BO_6 octahedron is capable of shifting towards one Ba-site doping ion (such as Nd^{3+} (1.27 Å) [5]) along cell-cube diagonal, which will diminish the internal deformation

of the TiO_6 octahedrons caused by donor and acceptor. The Raman charge effect disappears, as seen in BNTF [33]. When the size of Ti-site doping ion such as Eu^{3+} (0.947 Å) [5] is greater than that of Ti^{4+} (0.605 Å), for a self-compensation mode of $Eu_{Ba}^{\cdot} - Eu_{Ti}^{\prime}$ [36], the mobility of one Ti-site doping ion in the BO_6 octahedron is restricted and an internal deformation of the TiO_6 octahedrons caused by donor and acceptor may persist. The Raman charge effect is therefore present, as seen in $(Ba_{1-x/2}Eu_{x/2})(Ti_{1-x/2}Eu_{x/2})O_3$ [36]. As a matter of fact, the Ti-site dopants in doped $BaTiO_3$ where the Raman charge effect appears are relatively larger ions compared to Ti^{4+}, such as Nb^{5+} (0.64 Å [5]) [37] and Ca^{2+} (1.00 Å) [32]. The hexagonal $Ba(Ti_{1-y}Fe_y)O_{3-\delta}$ with smaller Fe^{3+} compared to Ti^{4+} does not show any Raman charge effect [33]. Thus, the Raman charge effect in BLTC is associated with the much larger ionic size of Ti-site Ca^{2+} compared to Ti^{4+}, rather than the disorder of La^{3+}/Ca^{2+} ions in orientations.

4.2. Dielectric-temperature stability

The dielectric-temperature stability of BLTC exhibited two features: (1) the Curie peak ($T_C = \sim 125\,^{\circ}C$) of $BaTiO_3$ could be not shifted by co-doping with La^{3+} (1.36 Å) and Ca^{2+} (1.00 Å); and (2) the Curie peak was almost completely suppressed. It can be sure that neither part of fine-grained microstructure [38–40] nor porosity [41] in BLTC was responsible for the suppression of the Curie peak of $BaTiO_3$. Recently, we found that the amphoteric doping behavior of Ba-site Ce^{3+} (1.34 Å) and Ti-site Ce^{4+} (0.87 Å) can induce an *In situ* diffuse phase transition at T_C of $BaTiO_3$ and led to a high-k behavior [42]. Thus, the dielectric-temperature stability of BLTC can be attributed to the formation of $La_{Ba}^{\cdot} - Ca_{Ti}^{\prime\prime} - La_{Ba}^{\cdot}$ defect complexes and the existence of much larger Ca^{2+} at the Ti site. La^{3+} at the Ba site contributes to the persistence of higher permittivity in an X7R range.

The samples with $x = 0.04$–0.06 had a higher tan δ relative to the sample with $x = 0.03$. This implies that with increasing doping levels, the formation of $La_{Ba}^{\cdot} - Ca_{Ti}^{\prime\prime} - La_{Ba}^{\cdot}$ defect complexes does not completely remove oxygen vacancies caused by the substitution of Ca^{2+} for Ti^{4+} [9,20,21], and the oxygen vacancies are apt to survive in the BLTC grain surface layers.

5. Conclusions

$(Ba_{1-x}La_x)(Ti_{1-x/2}Ca_{x/2})O_3$ ($0.03 \leqslant x \leqslant 0.06$) (BLTC) ceramics can be prepared at a lower temperature of 1400 °C by means of the formation of $La_{Ba}^{\cdot} - Ca_{Ti}^{\prime\prime} - La_{Ba}^{\cdot}$ defect complexes. All the BLTC samples are pseudo-cubic, which is marked by a symmetric (200) XRD peak indicative of cubicity and a sharp 308 cm^{-1} Raman band indicative of tetragonality. The unit cell volume (V_0) of BLTC increases linearly with x, satisfying Vegard's law. The V_0 of BLTC less than that of the tetragonal $BaTiO_3$ give evidence for the formation of $La_{Ba}^{\cdot} - Ca_{Ti}^{\prime\prime} - La_{Ba}^{\cdot}$ defect complexes. The aliovalent substitutions of La^{3+} at the Ba^{2+} site and Ca^{2+} at the Ti^{4+} site leads to a strong "Raman charge effect" marked by the 836 cm^{-1} band. Although the samples with $x = 0.04$, 0.05 and 0.06 satisfy X7R, X5R, and X8R specifications, respectively, the $x = 0.03$ sample because of its higher permittivity ($\varepsilon' = \sim 2000$) and lower loss (tan $\delta < 0.04$) can be considered as a novel dielectric for X7R applications. The formation of $La_{Ba}^{\cdot} - Ca_{Ti}^{\prime\prime} - La_{Ba}^{\cdot}$ defect complexes and the existence of much larger Ca^{2+} at the Ti site are responsible for the dielectric-temperature stability of BLTC.

Acknowledgements

This work was supported by the National Natural Science Foundation of China (No. 21271084), Projects of Jilin Provincial Science and Technology Department (No. 20121825) and International Science and Technology Cooperation (No. 20110710).

References

[1] A.F. Devonshire, Philos. Mag. 40 (1949) 1040–1063.
[2] M.L. Mulvihill, K. Uchino, L. Zhang, W.-W. Cao, Philos. Mag. B 74 (1996) 25–36.
[3] D. Hennings, A. Schnell, G. Simon, J. Am. Ceram. Soc. 65 (1982) 539–544.
[4] D.-Y. Lu, M. Sugano, W.-H. Su, T. Koda, Cryst. Res. Technol. 40 (2005) 703–708.
[5] R.D. Shannon, Acta Cryst. A 32 (1976) 751–767.
[6] V. Kumer, J. Joseph, I.P. Selvam, J. Ceram. Soc. Jpn. 113 (2005) 784–787.
[7] P.S. Dobal, A. Dixit, R.S. Katiyar, Z. Yu, R. Guo, A.S. Bhalla, J. Appl. Phys. 89 (2001) 8085–8091.
[8] A. Chen, Y. Zhi, J. Zhi, P.M. Vilarinho, J.L. Baptista, J. Euro, Ceram. Soc. 17 (1997) 1217–1221.
[9] L. Zhang, O.P. Thakur, A. Feteira, G.M. Keith, A.G. Mould, D.C. Sinclair, A.R. West, Appl. Phys. Lett. 90 (2007) 142914.
[10] T. Mitsui, W.B. Westphal, Phys. Rev. 124 (1961) 1354.
[11] R.K. Zheng, J. Wang, X.G. Tang, Y. Wang, H.L.W. Chan, C.L. Choy, X.G. Li, J. Appl. Phys. 98 (2005) 084108.
[12] L. Zhang, X. Wang, W. Yang, H. Liu, X. Yao, J. Appl. Phys. 104 (2008) 014104.
[13] T. Shimizu, D. Fu, H. Taniguchi, T. Taniyama, M. Itoh, Appl. Phys. Lett. 100 (2012) 102908.
[14] Z.Q. Zhuang, M.P. Hamer, D.M. Smyth, Mater. Res. Bull. 22 (1987) 1329–1335.
[15] P.S.R. Krishna, D. Pandey, V.S. Tiwari, R. Chakravathy, B.A. Dasannacharya, Appl. Phys. Lett. 62 (1993) 231–233.
[16] N.-H. Chan, D.M. Smyth, J. Am. Ceram. Soc. 67 (1984) 285–288.
[17] F.D. Morrison, D.C. Sinclair, A.R. West, J. App. Phys. 86 (1999) 6355–6366.
[18] D.M. Smyth, J. Electroceram. 9 (2002) 179–186.
[19] D. Li, A. Munirpallam, Subramanian, J. Solid State Sci. 2 (2000) 507–512.
[20] L. Zhang, L. Ben, O.P. Thakur, A. Feteira, A.G. Mould, D.C. Sinclair, A.R. West, J. Am. Ceram. Soc. 91 (2008) 3101–3104.
[21] N. Nasó, M. Prades, H. Beltrán, E. Cordoncillo, D.C. Sinclair, A.R. West, J. App. Phys. 97 (2010) 062907.
[22] F.A. Kröger, H.J. Vink, Relations between the concentrations of imperfections in crystalline solids, in: F. Seitz, D. Turnbull (Eds.), Solid State Physics, Academic Press, New York, 1956, p. 307.
[23] D.-Y. Lu, M. Sugano, M. Toda, J. Am. Ceram. Soc. 89 (2006) 3112–3123.
[24] A. Kerfah, K. Taïbi, A. Guehria-Laidoudi, A. Simon, J. Ravez, Solid State Sci. 8 (2006) 613–618.
[25] X. Diez-Betriu, J.E. Garcia, C. Ostos, A.U. Boya, D.A. Ochoa, L. Mestres, R. Perez, Mater. Chem. Phys. 125 (2011) 493–499.
[26] F.I.H. Rhouma, A. Dhahri, J. Dhahri, H. Helmabrouk, M.A. Balente, Solid State Common. 152 (2012) 1874–1879.
[27] R.Z. Chen, X.H. Wang, L.T. Li, Z.L. Gui, Mater. Sci. Eng. B 99 (2003) 298–301.
[28] C. Ma, X.H. Wang, R.Z. Chen, L.T. Li, Z.L. Gui, J. Electroceram. 21 (2008) 242–245.
[29] H.I. Hsiang, L.T. Mei, Y.J. Chun, J. Am. Ceram. Soc. 92 (2009) 2768–2771.
[30] D.-Y. Lu, X.-Y. Sun, M. Toda, J. Phys. Chem. Solids 68 (2007) 650–664.
[31] M. Kchikech, M. Maglione, J. Phys. Conden. Matter 6 (1994) 10159–10170.
[32] M.C. Chang, S.-C. Yu, J. Mater. Sci. Lett. 19 (2000) 1323–1325.
[33] D.-D. Han, D.-Y. Lu, X.-Y. Sun, J. Alloys Comp. 576 (2013) 24–29.
[34] G.E. Dieter, Mechanical Metallurgy, McGraw-Hill Book, London, 1988.
[35] Z. Yao, H. Liu, Y. Liu, Z. Wu, Z. Shen, Y. Liu, M. Cao, Mater. Chem. Phys. 109 (2008) 475–481.
[36] D.-Y. Lu, T. Ogata, H. Unuma, X.-C. Li, N.-N. Li, X.-Y. Sun, Solid State Ionics 201 (2011) 6–10.
[37] R. Farhi, M. El Marssi, A. Simon, J. Ravez, Euro. Phys. J. B 18 (4) (2000) 605–610.
[38] K. Kinoshita, A. Yamaji, J. Appl. Phys. 47 (1976) 371–373.
[39] A.J. Bell, A.J. Moulson, L.E. Cross, Ferroelectrics 54 (1984) 147–150.
[40] G. Arlt, D. Hennings, G. de With, J. Appl. Phys. 58 (1985) 1619–1625.
[41] D.-Y. Lu, T. Koda, H. Suzuki, M. Toda, J. Ceram. Soc. Jpn. 113 (2005) 721–727.
[42] D.-Y. Lu, D.-D. Han, Ceram. Int. 39 (2013) 9727–9730.